Chao Wen

In Situ **Observation of Current Generation in ZnO Nanowire Based Nanogenerators Using a CAFM Integrated into an SEM**

MASTER'S DEGREE FINAL PROJECT

Member of Prof. Dr. Eduard Llobet's Group

MASTER'S DEGREE IN NANOSCIENCE, MATERIALS AND PROCESSES: CHEMICAL TECHNOLOGY AT THE FRONTIER

UNIVERSITAT ROVIRA i VIRGILI

SOOCHOW UNIVERSITY

UNTO A FULL GROWN MAN

Tarragona

2019

In Situ Observation of Current Generation in ZnO Nanowire Based Nanogenerators Using a CAFM Integrated into an SEM

Chao Wen
Master Program in Nanoscience, Materials and Processes:
Chemical Technology at the Frontier 2018-2019
E-mail: chao.wen@estudiants.urv.cat

Supervisors: Eduard Llobet & Mario Lanza
Department of Electronic, Electrical and Automatic Engineering, Rovira i Virgili University, Avinguda Països Catalans 26, Tarragona, 43007, Spain

Abstract: Piezoelectric energy generators are promising systems which provide power for wireless electronic devices because they can harvest mechanical energy from the environment. In the last decades, piezoelectric nanogenerators such as zinc oxide (ZnO) nanowire-based nanogenerators have attracted much attention due to their small size and high current density. However, the origin of currents generated from ZnO nanowire remains unclear. In this report, we systematically characterize current generation in ZnO nanowire using a conductive atomic force (CAFM) microscope head mounted into the scanning electron micorscope (SEM) chamber. This set up can help us to monitor the ZnO nanowire bending process and record the *in situ* information of current generated at the same time. We find that currents generated during ZnO nanowire bending not only come from piezoelectric effect but also from contact potential and triboelectric effect. Since contact potential and triboelectric effect have been ignored in previous work, the power conversion effciency of piezoelectric nanogenerators has been overestimate. Our work helps to better understand the working mechanism of ZnO nanowire based piezoelectric nanogenerators. Moreover, this setup is very useful for other *in situ* study of nano-structured materials in the future.

Introduction

Wireless devices have become very interesting because they could be placed anywhere without cabling. For example, they could be used as biosensors attached to the skin [1]. Since wireless devices do not have cables to provide energy, they require one part inside of them to offer energy. This part can be a battery, which only has limited life time and needs to be recharged after a certain period of time; or this part can be an energy harvesting system. Energy harvesting is the process where environmental energy can be captured and stored for wireless devices [2]. Ambient energy such as thermal energy and solar energy could be harvested by solar cell and thermomagnetic generator [3-4], while mechanical energy could be harvested by electrostatic effect and piezoelectric effect [5-6]. One advantage of generators based on piezoelectric effect is that the power could be scalable up by combining single piezoelectric energy generator while the characteristic dimension of single generator could be scaled down to nanoscale [7]. And this is one of the reasons why ZnO nanowire based energy generators become very interesting.

The first characterization of ZnO nanowire was conducted by Wang's group in 2006 using a CAFM [8]. The bottom part of the single ZnO nanowire array is grounded and a resistor is applied in the circuit. The CAFM tip scans the ZnO nanowire in contact mode to bend ZnO nanowire and record the current generated during the bending process. In the next work of Wang's group, they reported the expected efficiency of the single ZnO nanowire is about 30% [9]. In order to verify Wang's work, M. Alexe et al. reproduced the experiment; however, they found that the measured signals might have different sources in addition to the piezoelectric effect [7]. In other words, the current origin generated during ZnO bending process is unclear. Apart from the unclear current origin, another issue that may affect the performance of ZnO nanowire is nanowire clustering. Nanowire clustering is still unavoidable although reasonably good vertical alignment can be achieved during the synthesis ZnO nanowire arrays [10]. In this case, it is quite difficult to determine whether the CAFM tip measures the current generated from on single ZnO nanowire or one ZnO nanowire cluster, which will result in an overestimation of power conversion efficiency (PCE). Moreover, ZnO nanowire cluster will lead to insufficient bending of ZnO nanowire, reducing the overall performance of ZnO nanowire arrays. For these reasons, it is important to find characterization techniques which can not only provide visualization of the ZnO nanowire bending process but also record *in situ* information of current generated in ZnO nanowire based nanogenerators.

One possible solution to realize the recording of combined information is a combination of different characterization techniques. For example, Agrawal's group realized the *in situ* observation of elastic modulus of ZnO nanowires by the integration of the microelectromechanical-system (MEMS) with transmission electron microscope (TEM) [11]. MEMS is used to electronically measure the applied load at nano-Newton resolution, while TEM provides the observation of continuous deformation of ZnO nanowire. However, this characterization technique requires a complex sample preparation. Moreover, although this setup can provide visualization of the ZnO nanowire bending, it can not be used to record the current generated during ZnO nanowire bending process.

In this report, we used for the first time the SEM-AFM (a CAFM head installed into the SEM chamber) setup to realize the *in situ* observation of current generation in ZnO nanowire based nanogenerators. With the help of this setup, we are able to reveal that the current generated during ZnO nanowire bending comes not only from piezoelectric effect, but also from contact potentials and triboelectric effects. This finding is important for understanding the working mechanism of ZnO nanowire based nanogenerators.

Experimental

<u>Growth of ZnO nanowire arrays</u>

We used the chemical hydrothermal method to synthesize ZnO nanowire arrays, including three steps: *i*) ZnO seed layer depostion, *ii*) nutrient solution preparation and *iii*) ZnO nanowire growth. Firstly, the silicon wafer was sequentially cleaned by acetone, ethanol and deionized water (10 minutes per step) with ultrasonic bath, then dried using a nitrogen gun. Then, a 5 nm thick ZnO seed layer was deposited onto the surface of silicon wafer using magnetron plasma sputtering (Kurt J. Lesker, PVD75). Secondly, 0.01 mol $Zn(NO_3)_2 \cdot 6H_2O$, 0.01 mol hexamethylenetetramine (HMTA) and 10 mL of ammonium hydroxide were diluted in 100 mL deoinzed water to prepare the nutrient solution. Thirdly, the nutrient solution was palced into a sealed teflon-lined stainless steel autoclave, and the sillicon wafer with ZnO seed layer was immersed into the nutrient solution. Then, the chemical hydrothermal synthesis of ZnO nanowire was conducted by placing the autoclave under 95 ^oC for 3 hours. And finally, the grown ZnO nanowire arrays were wased by deionized water and dried with the nitrogen gun.

SEM-AFM information

The SEM-AFM system, designed by Semilab GmbH in Germany, consists of a self-designed CAFM head installed into the vacuum chamber of a SEM from ZEISS and electronic components. The schematic of the setup is shown in Figure 1. The electronic components, such as the preamplifier, the laser diode and the detector, are situated in the vacuum chamber in hermetically encapsulated compartments.

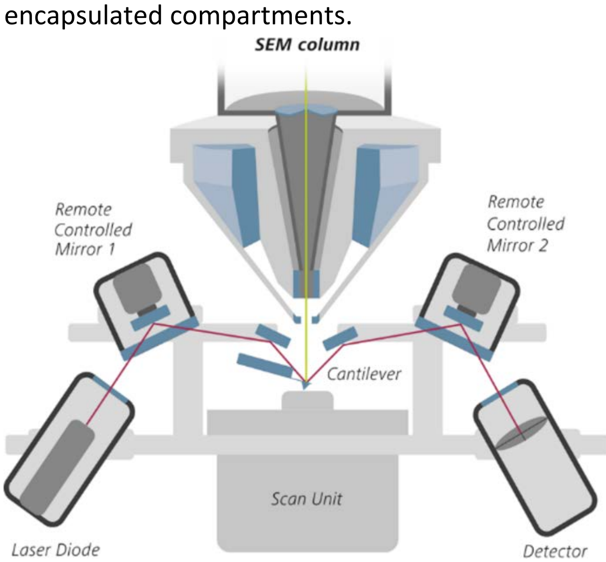

Figure 1. Schematic of the CAFM head integrated into the SEM with electronic components situated in the chamber.

The alignment of the laser path and the exchange of the cantilever and the sample can be obtained without breaking the vacuum, while the positioning of the CAFM tip to specific area can be achieved by a remote control. Therefore, this setup allows selecting which position of the sample the CAFM tip is about to land on and observing the movement of the CAFM tip during ZnO nanowire bending process. Figure 2 shows the SEM image of the CAFM tip landing on the ZnO nanowire array. In order to achieve the seamless operation of SEM and AFM, a single software interface is designed to operate both systems on one platform without clicking on tabs and windows [12]. In order to aviod the effect of electron beam on electrical signal during the measurement, the SEM electron beam can be switched off when necessary. The experiments were carried out in vacuum (at 10^{-6} Pa) at room temperature.

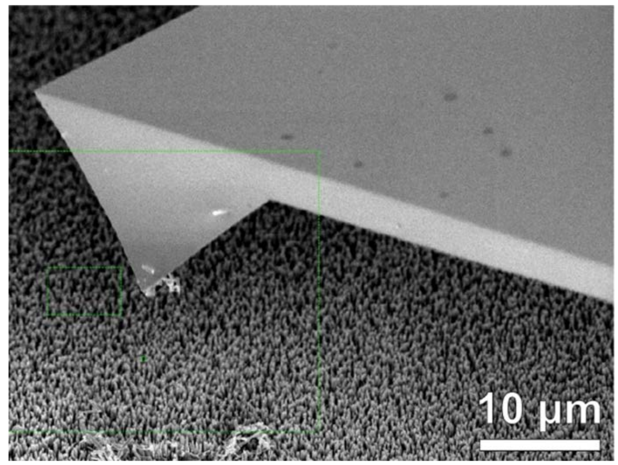

Figure 2. SEM image of a CAFM tip placed on the nanowire arrays.

Tip information

Two different types of CAFM tips were used to measure ZnO nanowire array: non-conductive Si tip and conductive Pt-Ir coated Si tip. After the smaple is fixed, the CAFM tip approaches the surface of ZnO nanowire array and starts to measure. The non-conductive Si tip can be used in tapping mode to measure the topography of ZnO nanowire array while the conductive Pt-Ir coated Si tip can be used in contact mode to measure the topography and current simultaneously.

Results

Morphological characterization of ZnO nanowire

The top view SEM image and topographic map of ZnO nanowire arrays are shown in Figures 3a and 3b. In order to obtain the topographic map of the sample, a non-conductive Si tip and a low contact fore were used in tapping mode, which could avoid ZnO nanowire bending. This method provides a clear-cut image without horizontal lines, indicating no ZnO nanowire bending during the measurement [13]. The absence of ZnO nanowire bending could be further prooved by supplementary video 1. As shown in Figure 3a, the diameter of ZnO nanowire is around 250 nm, similar with that observed in Figure 3b. The sharp and stepped top end demonstrates the high ceystallinity od ZnO nanowires.

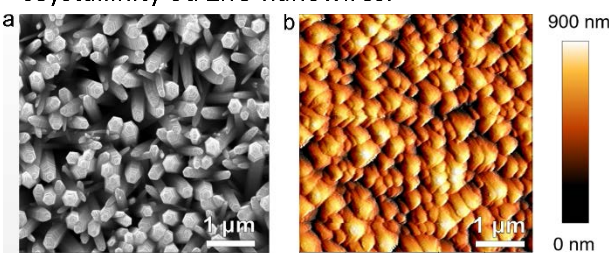

Figure 3. (a) Top view SEM image of the ZnO nanowire array. (b) AFM topographic image of ZnO nanowire array collected in tapping mode by a non-conductive Si tip.

Electronic characterization of ZnO nanowire

Figures 4a and 4b show the topographic map and current map of ZnO nanowire array collected simultaneously in contact mode using a conductive Pt-Ir coated Si tip. As shown in Figure 4a, the diameter of ZnO nanowire is around 500 nm, larger than that observed in Figure 3b collected in tapping mode. This is related to the larger apex radius of conductive Pt-Ir coated Si tip used in contact mode. Compared with the non-conductive Si tip, the conductive Pt-Ir coated Si tip has a less sharp shape and could not penetrate into the narrow gap between ZnO nanowires, leading to a larger ZnO nanowire diameter. During the measurement, although the conductive tip was in contact with the surface of the sample, it is confirmed by SEM that ZnO nanowire did not bend. It is interesting that, although ZnO nanowire didn't bend, current spots were detected as shown in Figure 4b. However, the current generated here could not be related to piezoelectric effect as the ZnO nanowire didn't bend. If the current observed in Figure 4b is not related to piezoelectric effect, it may be related to SEM lectron gun.

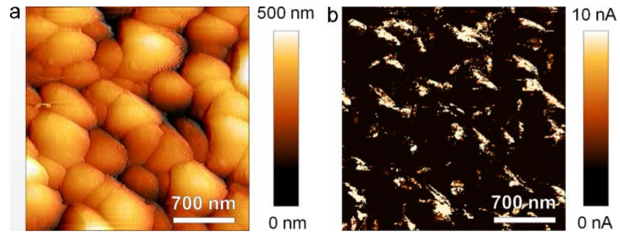

Figure 4. (a) AFM topographic image of ZnO nanowire array collected in contact mode by a conductive Pt-Ir coated Si tip. The tip is in contact with the surface of the sample without ZnO nanowire bending, which could be confirmed by SEM. (b) AFM current map of ZnO nanowire array collected simultaneously without a bias voltage applied.

In order to verify this hypothesis, some additional experiments have been conducted. First, the SEM electron gun was switched off and the experiments were repeated, in which similar current signals were observed. Second, the same experiments were conducted in a standard CAFM, and similar current images were obtained. And third, no current was detected when the CAFM tip is placed statically on a ZnO nanowire, which demonstrates that the current is related to CAFM tip movement instead of the SEM gun. In conclusion, the influence of the SEM electron gun on the current collected by the CAFM tip has been ruled out. Therefore, the only reasonable interpretation is that it may be related to the contact potentials or triboelectric effects generated during the tip movement and the tip/nanowire contact [14-15]. For clarity, contact potential is defined as the electrostatic potential between two different electrically conductive or semiconducting materials when they are brought into contact [16], and triboelectric effect is defined as the electrification of some materials when they are in frictional contact with another material [17].

Current origin of ZnO nanowires

In order to find out the current origin during ZnO nanowire bending, the current vs. lateral distance (I-X) curve was collected by a Pt-Ir coated Si tip. In order to carry out this experiment, the feedback was switched off so that the tip could be moved at a certain height without self-reaction. The schematics of the experiment at five different stages are shown in figure 5a while the SEM images at different steps are shown in figure 5b correspondingly. Figure 5c shows the I-X curve at different stages.

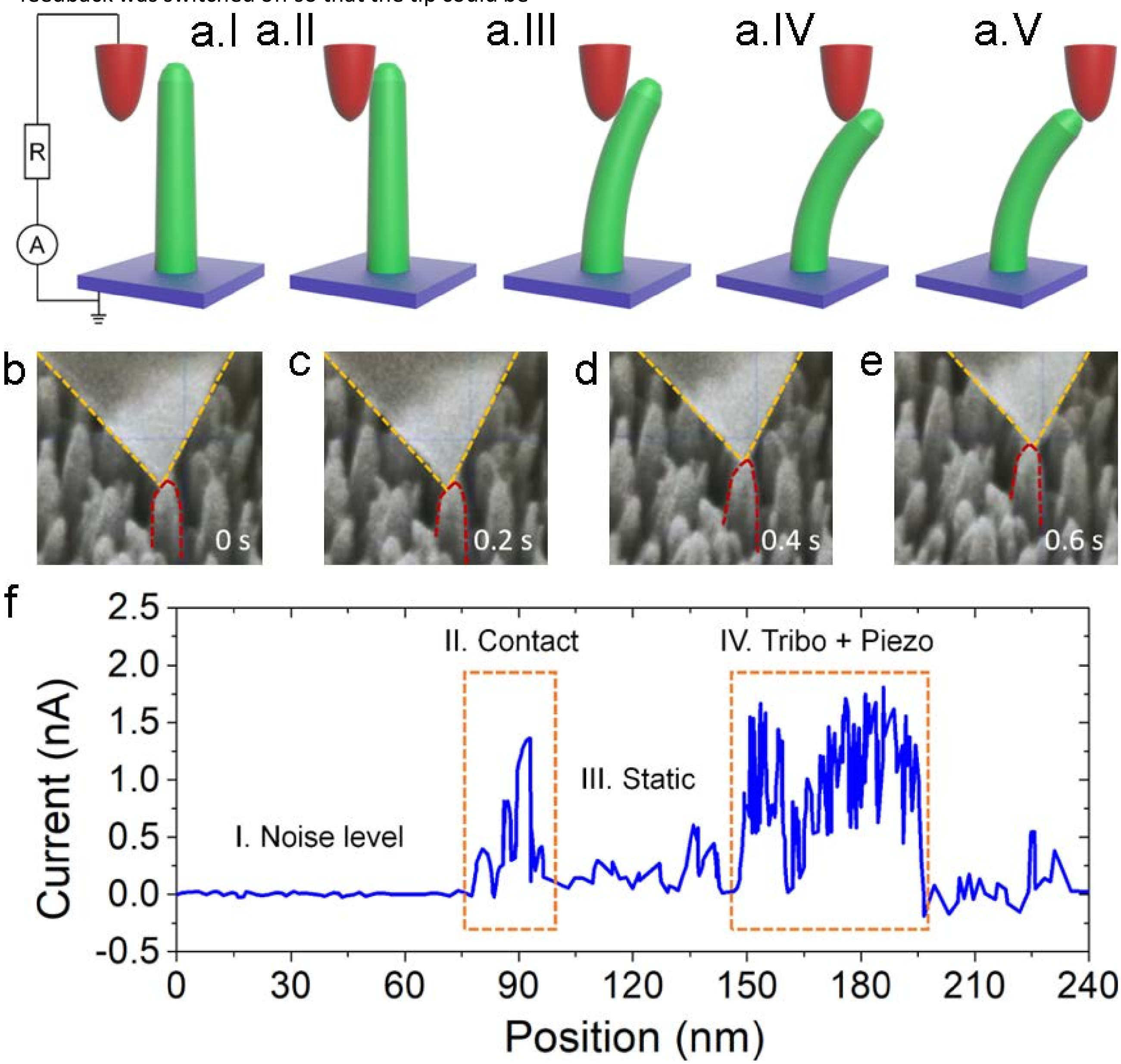

Figure 5: (a) Schematics of I-X curve collected at five different stages. (b) SEM images at four steps during ZnO nanowire bending, corresponding to what shown in Figure 5a. The detailed information of the whole ZnO nanowire bending process is shown in supplementary video 2. (c) I-X curve showing the current signals at different steps.

As shown in the I-X curve, the current detected is firstly at noise level (see Figure 5f.I) when CAFM tip is far away from ZnO nanowire (see Figure 5a.I). The noise level (around 50 pA) is slightly higher than that (around 0.2 pA) in other experiments using CAFM [18] due to the existence of SEM electron beam. With the movement of CAFM tip, several current peaks appear at around 75 nm (see Figure 5f.II) in I-X curve when the tip touches the ZnO nanowire (see Figure 5a.II). It should be highlighted that current peaks observed here can not be related to piezoelectric effect as both SEM image (Figure 5b) and supplmentary video 2 indicate that ZnO did not bend. Therefore, the only feasible explanation is that the current peaks collected between 75 nm and 100 nm is associated with contact potentials generated during tip/nanowire contact. After the tip touches the ZnO nanowire, the ZnO nanowire starts to bend (see Figures 5a.III and 5c), however, almost no current is collected from 100 nm to 150 nm (see Figure 5f.III). This may be caused by the reversed Schottky barrier between the elongated nanowire side and metal coated CAFM tip, resulting in no piezo-current output. Another possible reason may be no relative sliding along the ZnO nanowire interface as static friction causes the tip to stuck to the contact point. After this, a wide range of current peaks appear at around 150 nm (see Figure 5f.IV) in the I-X curve, which indicates that the CAFM tip slides along nanowire/tip interface (see Figure 5a.IV and 5d), reaches the compression side of ZnO nanowire then detaches the nanowire at around 200 nm (see Figure 5a.V). At around 150 nm, CAFM tip starts to slide over the nanowire surface and some current can be detected even with the existence of a reverse Schottky barrier. Therefore, the current generated here is independent of piezoelectric effect but may be related to the triboelectric effect. When CAFM tip moves to the compressed side of ZnO nanowire, the nanowire/tip contact becomes a forward Schottky barrier, resulting in the discharge of piezoelectric potential. It may be suspected that the current origin changes from triboelectric effect to piezoelectric effect near 160 nm where currents return to zero. However, it is very difficult to distinguish triboelectric effect from piezoelectric effect in the current region (Figure 5f.IV). Moreover, these two effects may happen simultaneously, since the CAFM tip may also slide over the compressed side of ZnO nanowire when scanning. As a result, current peaks observed in Figure 5f.IV can be related to both triboelectric effect and piezoelectric effect and this is the reason why there is no distinction in this region. Apart from the currents observed in I-X curve, the distance between the contact point and separate point is also very interesting. With the contact point at 75 nm and separate point at 200 nm, the distance is 125 nm, at the same order than nanowire diameter, further validating this experiment.

Conclusions

In conclusion, the current generation in ZnO nanowire has been systematically characterized using a CAFM head intergrated into the SEM chamber. This setup not only provides visualization of ZnO nanowire bending process but also records the *in situ* information of current generated. Through the combined information, we are able to reveal three origins of the currents generated during ZnO nanowire bending: piezoelectric effect, contact potential and triboelectric effect. Moreover, we could distinguish these three types of currents using I-X curve. It should be highlighted that this finding can only be achieved through this experimental setup. The setup described here could be very useful for other *in situ* study of nano-structured materials.

Acknowlegement

This work has been done as a cooperation of Prof. Eduard Llobet from Universitat Rovira i Virgili and Prof. Mario Lanza from Soochow University. It has been supported by the Young 1000 Global Talent Recruitment Program of the Ministry of Education of China, the Ministry of Science and Technology of China (grant BRICS2018-211-2DNEURO), the National Natural Science Foundation of China (grants 61502326, 41550110223, 11661131002, 61874075), the Jiangsu Government (grant BK20150343), the Ministry of Finance of China (grant SX21400213) and the Young 973 National Program of the Chinese Ministry of Science and Technology (grant 2015CB932700). The Collaborative Innovation Center of Suzhou Nano Science & Technology, the Jiangsu Key Laboratory for Carbon-Based Functional Materials & Devices, the Priority Academic Program Development of Jiangsu Higher Education Institutions, and the 111 Project from the State Administration of Foreign Experts Affairs are also acknowledged. Additional support has been from the Engineering and Physical Sciences Research Council, UK under grant number EP/K01739X/1, Leverhulme Trust under grand number RPG-2016-135, and The Worshipful Company of Scientific Instrument Makers.

References

[1] M.L. Johnson, J. Wan, S. Huang, Z. Cheng, V. A. Petrenko, D.-J. Kim, I-H. Chen, J. M. Barbaree, J. W. Hong, and B. A. Chin. Sensors and Actuators A: Physical **2008**, 144, 38.

[2] U. Guler, M.S. Sendi, and M. Ghovanloo. 2017 IEEE 60th International Midwest Symposium on Circuits and Systems (MWSCAS).

[3] G. Li, R. Zhu, and Y. Yang. Nature Photonics **2012**, 6, 153.

[4] M. Ujihara, G.P. Carman, and D.-G. Lee. Applied Physics Letters **2007**, 91, 093508.

[5] H. Xiao, G. Chen, X. Chen, and Z. Chen. Scientific rReports **2017**, 7, 8443.

[6] Y. B. Jeon, R. Sood, J-H. Jeong, and S-G. Kim. Sensors and Actuators A: Physical **2005**, 122, 16.

[7] M. Alexe, S. Senz, M. A. Schubert, D. Hesse, and U. Gösele. Advanced Materials **2008**, 20, 4021.

[8] Z.L. Wang and J. Song, Science **2006**, 312, 242.

[9] X. Wang, J. Song, J. Liu, and Z. L. Wang. Science **2007**, 316, 102.

[10] C. Pan, J. Hu, E. G. Gutierrez, M. T. Hoang, H. Duan, J. Yvonnet, A. Mitrushchenkov, G. Chambaud, and M. Lanza. Journal of Materials Chemistry C **2016**, 4, 3646.

[11] R. Agrawal, B.P1eng, E. E. Gdoutos, and H. D. Espinosa. Nano Letters **2008**, 8, 3668-3674.

[12] Semilab GmbH, ZEISS integrated Atomic Force Microscope, Accessed June 6th 2019, https://www.semilab.hu/category/products/sem-afm.

[13] M. Lanza, M. Reguant, G. Zou, P. Lv, H. Li, R. Chin, H. Liang D. Yu, Y. Zhang, Z. Liu, H. Duan. Advanced Materials Interfaces **2014**, 1, 1300101.

[14] S. Kitamura, K. Suzuki, and M. Iwatsuki. Applied Surface Science **1999**, 140, 265.

[15] S.I Kitamura, and M. Iwatsuki. Applied Physics Letters **1998**, 72, 3154.

[16] E. Guptill, M. Calkin, and M. Jericho. Canadian Journal of Physics **1972**. 50, 2967.

[17] Z.L. Wang, ACS Nano **2013**. 7, 9533.

[18] M. Lanza, M. Porti, M. Nafria, X. Aymerich, G. Benstetter, E. Lodermeier, H. Ranzinger et al. IEEE Transactions on Nanotechnology **2010**, 10, 344.